Universality of phloem transport in seed plants

KÅRE HARTVIG JENSEN[1]*, JOHANNES LIESCHE[2]*, TOMAS BOHR[1] & ALEXANDER SCHULZ[2]

[1]*Department of Physics, Center for Fluid Dynamics, Technical University of Denmark, DTU Physics Building 309, DK-2800 Kongens Lyngby, Denmark and* [2]*Department of Plant Biology and Biotechnology, University of Copenhagen, Thorvaldsensvej 40, DK-1871 Frederiksberg C, Denmark*

ABSTRACT

Since Münch in the 1920s proposed that sugar transport in the phloem vascular system is driven by osmotic pressure gradients, his hypothesis has been strongly supported by evidence from herbaceous angiosperms. Experimental constraints made it difficult to test this proposal in large trees, where the distance between source and sink might prove incompatible with the hypothesis. Recently, the theoretical optimization of the Münch mechanism was shown to lead to surprisingly simple predictions for the dimensions of the phloem sieve elements in relation to that of fast growing angiosperms. These results can be obtained in a very transparent way using a simple coupled resistor model. To test the universality of the Münch mechanism, we compiled anatomical data for 32 angiosperm and 38 gymnosperm trees with heights spanning 0.1–50 m. The species studied showed a remarkable correlation with the scaling predictions. The compiled data allowed calculating stem sieve element conductivity and predicting phloem sap flow velocity. The central finding of this work is that all vascular plants seem to have evolved efficient osmotic pumping units, despite their huge disparity in size and morphology. This contribution extends the physical understanding of phloem transport, and will facilitate detailed comparison between theory and field experiments.

Key-words: long-distance transport; Münch mechanism; phloem; scaling; sieve elements; sugar; trees.

INTRODUCTION

Vascular transport of photoassimilates in plants from source to sink takes place in sieve elements (SEs). These specialized cells of the phloem form a continuous network running throughout the plant. The most widely accepted mechanism for phloem transport is the osmotic pressure-driven mass flow as proposed by Münch in the 1920s (Münch 1930). According to Münch, sugar produced in the leaves generates an osmotic pressure which drives a flow of water and sugar from source to sink, in accordance with the basic needs of the plants (Fig. 1a).

Correspondence: A. Schulz. e-mail: als@life.ku.dk

*These authors contributed equally to this work.

There is considerable knowledge of phloem transport in herbaceous angiosperms, where a large number of studies have contributed to our view on the mechanism of loading, translocation and unloading in this plant group (Holbrook & Zwieniecki 2005). Recent work involving translocation velocity measurements (Windt *et al.* 2006; Jensen *et al.* 2011), theoretical modelling and microfluidic model experiments (Jensen *et al.* 2009, 2011) have shown that the phloem vascular system of herbaceous angiosperms is geometrically optimized for rapid translocation, and that the Münch mechanism is sufficient to account for the observed translocation rates (Jensen *et al.* 2011). A relevant question is, whether this is also universally the case in trees, in particular in gymnosperms, which have not been considered so far.

All measurements of sap flow velocity in gymnosperm trees, except one (Willenbrink & Kollmann 1966), give a significantly slower speed compared with woody angiosperms (Crafts & Crisp 1971). Differences in methodology hinder the generalization of experimental results but direct comparison with identical experimental set-ups showed the same velocity difference (Thompson *et al.* 1979; Dannoura *et al.* 2011). Typical translocation velocities found in angiosperm are of the order 1 m h⁻¹ (Windt *et al.* 2006; Mullendore *et al.* 2010; Jensen *et al.* 2011), while observed velocities in gymnosperms typically are two to five times slower (Crafts & Crisp 1971; Thompson *et al.* 1979; Plain *et al.* 2009; Dannoura *et al.* 2011). Given the fact that the tallest trees are gymnosperms and that their SE anatomy with endoplasmic reticulum-obstructed sieve pores (Schulz 1992) appears incompatible with Münch pressure flow (Turgeon 2010), some authors have speculated that the transport process in gymnosperms may differ fundamentally from that found in angiosperms (Crafts 1939; Kollmann 1975; Liesche, Martens & Schulz 2011), although indirect experimental evidence suggests otherwise (Münch 1930; Watson 1980; Sevanto *et al.* 2003).

Despite the progress in theoretical modelling of Münch flow and agreement with experimental data from herbaceous plants, fundamental questions about phloem transport in both angiosperm and gymnosperm trees remain. Experimental data on transport speed, osmotic potential and conductivity are still scarce (Knoblauch & Peters 2010). The largest plants where phloem sap velocity was measured were a 4 m poplar [~0.7 m h⁻¹ (Windt *et al.* 2006)] and several beech (0.22–1.21 m h⁻¹), oak (0.36–1.02 m h⁻¹) and pine trees (0.09–0.21 m h⁻¹) of 8–10 m height (Dannoura
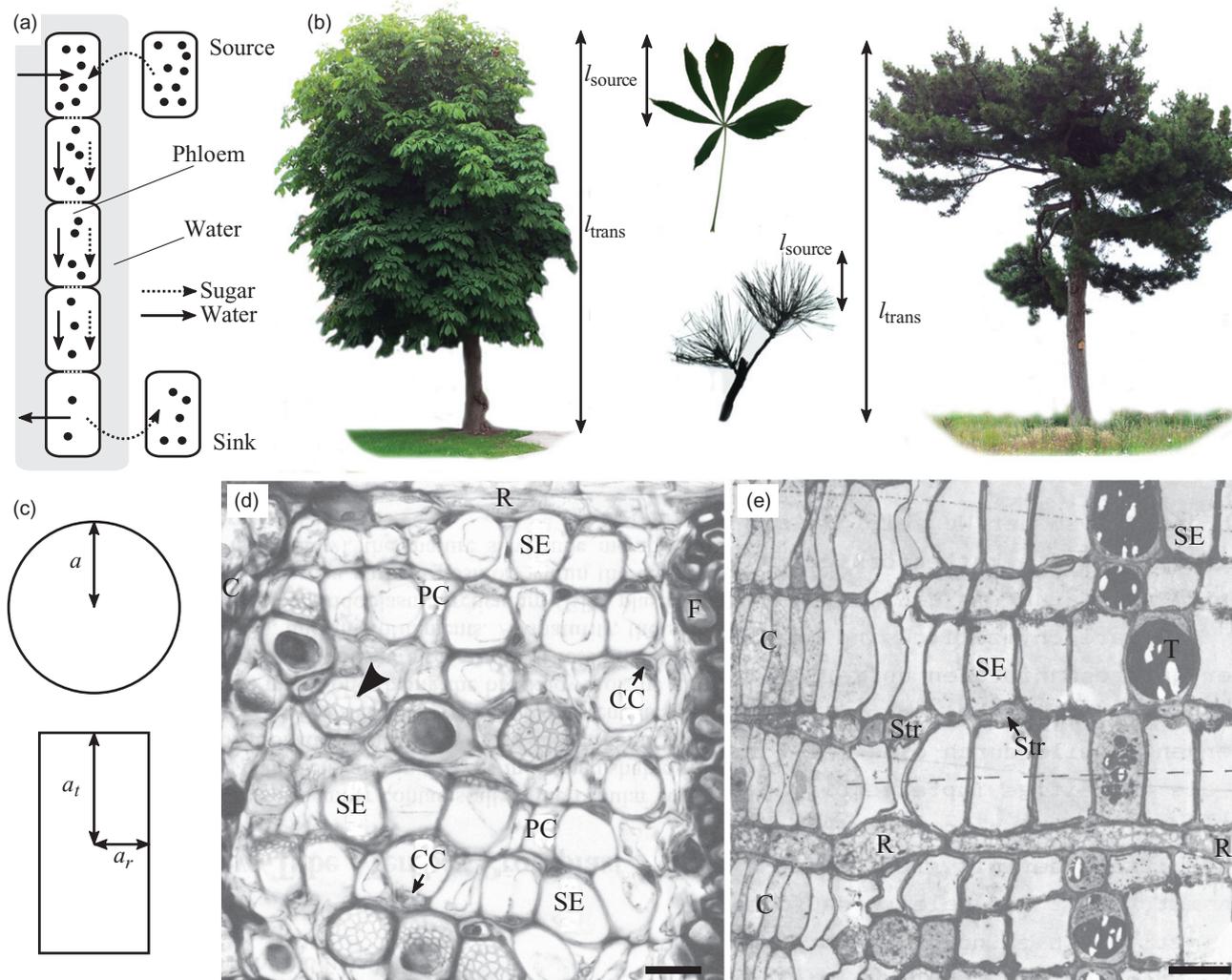
Figure 1. Aspects of plant anatomy relevant to phloem transport. (a) Schematic sketch of sugar translocation in plants according to the Münch hypothesis. In the source leaves, sugar (black dots) produced by photosynthesis is delivered into the phloem. Because of osmosis, the high concentration of sugar creates a flow of water across the semipermeable cell membrane from the surrounding tissue into the phloem. This in turn pushes the water and sugar already present forward, thereby creating a bulk flow from sugar source to sugar sink. At the sink, for example, the root, removal of sugar from the phloem causes the water to leave the cells because the osmotic driving force is no longer present. The loading and unloading processes are indicated by curved arrows. (b) Macroscopic parameters of phloem transport. Stem length l_{trans} and leaf length l_{source} indicated for an angiosperm (left and top middle) and gymnosperm (right and bottom middle). (c) Schematic sketch of sieve element (SE) geometry. In cross section, angiosperm SEs (top) are typically circular with radius a, while gymnosperm SEs are rectangular with tangential half width a_t and radial half width a_r. (d) and (e) Cross sections of secondary phloem in the stem of mature trees. Stem phloem consists of the conducting SEs, the companion cells (CC) in case of angiosperms (d) and Strasburger cells (Str) in case of gymnosperms (e), axially arranged ray parenchyma cells (R), fibres (F), parenchyma cells (PC) and sometimes tannin cells (T). In most species, only a part of the current year's phloem at the cambium (C) is functional. The arrowhead indicates a simple sieve plate, typical for angiosperm phloem. Scale bars = 20 µm; (d) secondary phloem of *Robinia pseudoacacia* adapted from Evert (1984); (e) secondary phloem of *Picea abies* adapted from Schulz & Behnke (1987).

et al. 2011); all species can easily reach heights of more than 20 m. If the observed transport velocity is representative for all exemplars, then an increased osmotic potential and/or higher sieve tube conductivity would be needed to offset the stem length effect. Despite the inaccessibility of the phloem to measurement of osmotic pressure and therefore lack of direct evidence (Millburn & Kallarackal 1989), it is now assumed that phloem pressure does not scale with plant height (Turgeon 2010). The measurement of key features of the SE anatomy should allow estimation of the conductivity and therefore answer the question if tall trees have the potential to transport with similar velocities observed in small trees and herbaceous plants.

METHODS

Theoretical analysis of the Münch pressure-flow mechanism

The most widely accepted mechanism for phloem transport is the osmotically driven pressure flow proposed by Münch

Table 1. Nomenclature

Name	Symbol	Value	Unit	Reference
SE radius, effective osmotic radius	a		m	
SE half width	a_r		m	
SE half height	a_t		m	
SE cross-sectional area	A		m^2	
Geometric factor	G	16 (circular), 3 (rectangular)		
Conductivity	k		m^2	
Membrane permeability	L_p	5×10^{-14}	m Pa^{-1} s^{-1}	(Thompson & Holbrook 2003b)
Sink length	l_{sink}		m	
Source/leaf length	l_{source}		m	
Stem/translocation length	l_{trans}		m	
Number of pores in membrane	N			
Resistance	R		(Pa s)/m^3	
Osmotic pressure difference	Δp	0.7	MPa	(Turgeon 2010)
Velocity	u		m s^{-1}	
Material factor	V	$16L_p\eta$	m	
Material factor	W	$3L_p\eta(1+\delta)/(\delta-0.63)$	m	
SE aspect ratio	$\delta = \dfrac{a_t}{a_r}$	$\simeq 2$		
Viscosity	η	2×10^{-3}	Pa s	(Thompson & Holbrook 2003b)
Membrane thickness	κ		m	
Membrane pore radius	ρ		m	
Membrane pore covering fraction	ϕ			
Membrane area	Ω		m^2	

SE, sieve element.

in the 1920s (Münch 1930). According to Münch, sugar produced in the leaves generates an osmotic pressure which drives a flow of water and sugar from source to sink, as sketched in Fig. 1a. The quantitative description of this translocation process falls in two categories: one (1) which uses solutions of the detailed equations governing fluid flow and solute transport (see, e.g. Thompson & Holbrook 2003b; Jensen *et al*. 2009; Pickard & Abraham-Shrauner 2009; Jensen *et al*. 2011); and another (2) which uses high level resistance models (see, e.g. Minchin, Thorpe & Farrar 1993) to characterize the flow. Here, we use a type of resistor model to describe the flow. Note that Jensen *et al*. recently showed a direct correspondence between certain type (1) and (2) models (Jensen *et al*. 2011).

The flow velocity *u* (for a list of symbols, see Table 1) at which the dissolved sugar is moving depends on the magnitude of the osmotic pressure difference Δp between source and sink and on the hydraulic resistance *R* of the translocation pathway

$$u = \frac{1}{A}\frac{\Delta p}{R} \qquad (1)$$

where *A* is the cross-sectional area of the SE (Jensen *et al*. 2011). The combined resistance experienced by the liquid as it moves along the phloem translocation pathway can be divided in three parts corresponding to the resistance in the leaf (source), stem (translocation) and root (sink) regions, as sketched in Fig. 1a:

$$R = R_{source} + R_{trans} + R_{sink} \qquad (2)$$

The magnitude of these three resistance components depends on the macroscopic size of the plant, in particular leaf length and stem length (Fig. 1b), the microscopic geometry of the SEs, and on the material properties of the semipermeable cell membrane and the sugar solution.

In this analysis, we ignore differences in the mode of phloem loading and unloading of sugars, which might be symplasmic or apoplasmic, active or passive (Rennie & Turgeon 2009). In any case, source organs are identified by high sugar concentrations and sink organs by high sugar consumption. This leads to an effective osmotic pressure difference Δp between source and sink and water influx and efflux in source and sink, respectively (see Fig. 1a).

SEs are predominantly found in two different shapes: cylindrical, typical of angiosperms, and cuboidal, of rectangular cross section, often found in gymnosperm trees (Fig. 1c,d,e). Here, we examine the case of cylindrical SEs in detail and only state results for cuboids, which are studied more carefully in Appendix A. For cylindrical SEs, the stem resistance is approximately that of a cylindrical tube $R_{trans} = \dfrac{8\eta l_{trans}}{\pi a^4}$, where η is the viscosity of the liquid, l_{trans} is the length of the stem, and *a* is the radius of the SE (Fig. 1c). The cross-sectional area is simply $A = \pi a^2$. The number and size of sieve pores connecting adjacent SEs are also believed to play a role (Mullendore *et al*. 2010), and may increase the effective viscosity of the liquid significantly (Thompson & Holbrook 2003b), but for simplicity we will not take this into account in the present analysis. As the length scales for leaves and roots are smaller than the translocation (stem) length, we assume that the resistance of the

source and sink regions is dominated by the osmotic resistance through surface area, that is $R_{source} = \dfrac{1}{2\pi a L_p l_{source}}$ and $R_{sink} = \dfrac{1}{2\pi a L_p l_{sink}}$ where L_p is the permeability of the semipermeable membrane. In terms of osmotic water transport, the permeability of the plasma membrane is determined by aquaporins (see Appendix B). From Eqns 1 and 2, we arrive at a simple expression for the velocity u as a function of the geometric and material parameters of the problem

$$\frac{u(a, l_{source}, l_{trans}, l_{sink})}{2L_p \Delta p} = \frac{a^2 l_{source} l_{sink}}{V l_{source} l_{trans} l_{sink} + a^3 (l_{source} + l_{sink})} \quad (3)$$

where we introduced the short-hand notation $V = 16 L_p \eta$. From Eqn 3 we recover several results found in the phloem literature, for example, that the transit time of a single sugar molecule $t = \dfrac{l_{trans}^2}{u}$ scales as l_{trans}^2 when l_{trans} is very large as found numerically by Thompson and Holbrook (Thompson & Holbrook 2003a). It is apparent from Eqn 3 that the translocation velocity u has a maximum as a function of cell radius a for fixed source, translocation and sink lengths when $a = a^*$, where

$$a^{*3} = 2V \frac{l_{source} l_{trans} l_{sink}}{l_{source} + l_{sink}} = 2V \frac{l_{trans}}{l_{source}^{-1} + l_{sink}^{-1}} \quad (4)$$

At this value of the radius, the osmotic pumping mechanism is operating at its maximum capacity. Inserting $a = a^*$ into (3) gives the optimal speed

$$\frac{u(a^*, l_{source}, l_{trans}, l_{sink})}{2L_p \Delta p} = K l_{trans}^{-1/3} \left(l_{source}^{-1} + l_{sink}^{-1} \right)^{-2/3} \quad (5)$$

where $K = 3^{-1} 2^{2/3} V^{-1/3}$. If we assume that the sink length l_{sink} (e.g. the length of the roots) is always larger than the source length (the leaves), the largest velocity is actually found when $l_{sink} \gg l_{source}$, where the right hand side of (5) gives $K l_{trans}^{-1/3} l_{source}^{2/3}$. In the case $l_{source} = l_{sink}$ the right hand side, however, gives practically the same result, being simply a factor $2^{-2/3} \approx 0.8$ lower, so the precise choice of the ratio of these length scales is unimportant. In the following, we thus assume that $l_{source} = l_{sink}$ and have for the optimum radius that

$$a^{*3} = 16 L_p \eta l_{source} l_{trans} \quad (6)$$

a result first found by Jensen *et al.* (2011).

It is interesting to note that the optimality condition (4) means that $R_{trans} = \frac{1}{2}(R_{source} + R_{sink})$, that is, that optimality sets the resistance through the stem to the mean resistance of the source and the sink.

For a rectangular cell (see Appendix A), we find for the optimized radius (when $l_{source} = l_{sink}$)

$$a^{*3} = 3 L_p \eta l_{source} l_{trans} \quad (7)$$

where the effective osmotic 'Münch' radius of the cuboidal cells is given by $a = a_r \left(\dfrac{a_t - 0.63 a_r}{a_t + a_r} \right)^{1/3}$. Here, a_r and a_t are the half width and half height of the cells, respectively (see Fig. 1c). Combining Eqns 6 and 7 we can write a general equation for the optimized 'Münch' radius a^* valid in both geometries:

$$a^{*3} = G L_p \eta l_{source} l_{trans}. \quad (8)$$

Here, G is a geometric factor depending only on the shape of the cell (with the value 16 for cylindrical cells and 3 for cuboidal cells). Under the assumption that plants are optimized for rapid phloem transport, Eqn 8 puts a constraint on the relative size of the various plant organs: cell radius a, stem length l_{trans} and leaf length l_{source}. The product of the membrane permeability L_p and liquid viscosity η is also a length scale, related to the hydrodynamic size and density of the pores in the semipermeable membrane (see Appendix B). In this way, Eqn 8 directly couples the macroscopic and microscopic structures of the plant.

Conductivity

Another equivalent formulation of the Münch flow Eqn 1 can be given in terms of the hydraulic conductivity k:

$$u = \frac{k}{\eta} \frac{\Delta p}{l_{trans}} \quad (9)$$

where there is an inverse relation between conductivity and resistance, cf. Eqn 1, $k = \dfrac{\eta l_{trans}}{AR}$. With Eqns 3 and A4, the conductivity can be calculated directly from Eqn 9 as $k = \dfrac{u \eta l_{trans}}{\Delta p}$. We note that while it generally depends on the geometric and material parameters of the problem, it does not depend on the pressure drop Δp, as $u \propto \Delta p$. The conductivity k gives a measure of how well the plant is able to conduct fluid flow, and is commonly used in quantitative studies of transport both in phloem (see, e.g. Thompson & Holbrook 2003b or Mullendore *et al.* 2010) and in xylem (Becker, Tyree & Tsuda 1999). Compared with Eqn 1, it uses the average pressure drop per unit length $\Delta p / l_{trans}$ rather than the absolute pressure difference between source and sink Δp to characterize the flow, thus allowing for a direct comparison of the hydraulic properties of plants of different heights.

Experimental methods

SE radii of secondary phloem, leaf size and stem size (given in Table 2) for 32 angiosperm species and 38 gymnosperm species were obtained from the literature (Chang 1954a,b; Esau 1969; Schulz & Behnke 1987; Jensen *et al.* 2011) and from samples taken in the field. In case a literature source did provide a value for SE radius but not for leaf and stem size, average values for these two measures were derived from online references.

Table 2. Plant data used in this study with a tree (T), shrub (S) and herbaceous (H) life forms. Values for leaf length (l_{source}), stem length (l_{trans}) and sieve element geometry (SE geometry, see Fig. 1c) were collected in the field or obtained from the literature as indicated in the reference column. In cases where leaf and/or stem length were not provided in the literature, values following general knowledge were obtained from online databases. SE cross-sectional area A, effective osmotic radius a, G $l_{source}l_{trans}$, conductivity k and translocation velocity u were calculated as described in the text and figure captions. Standard deviations are given when available

Species	Life form	l_{source} [cm] (1)	l_{trans} [m] (2)	SE geometry: a or (a_t);(a_r) [μm] (3)	Reference	A [1000 μm²]	a [μm]	G l_{source} l_{trans} [m²]	k [μm²]	u [μm s⁻¹]
Gymnosperms										
Abies balsamea (L.) Mill.	T	2.3 ± 0.8	17 ± 3	(10 ± 5);(14 ± 4)	Chang 1954a (3)	560	6.8	1.2	2.8	58.3
Abies alba Mill.	T	2.4 ± 0.6	45 ± 5	(5.6 ± 0.7);(10.2 ± 1.8)	Schulz & Behnke 1987 (3)	230	4.2	3.2	4.7	36.5
Abies grandis (Dougl.) Lindl.	T	4.5 ± 1.5	55 ± 15	(10 ± 2.5);(19 ± 9)	Chang 1954b (3)	760	7.6	7.4	10	65.1
Chamaecyparis obtusa	T	0.2 ± 0.04(s)	8.5 ± 0.9	(8.5 ± 1.4);(12.8 ± 2.3)	This study (1, 2, 3)	440	6	0.051	0.16	6.77
Chamaecyparis thyoides (L.)	T	0.30 ± 0.10(s)	24 ± 4	(7.5)(20)	Chang 1954b (3)	600	6.2	0.22	0.63	9.2
Cryptomeria japonica	T	1.1 ± 0.2	16 ± 1.6	(6.7 ± 1.2);(14.1 ± 2.3)	This study (1, 2, 3)	380	5.2	0.53	1.6	35.8
Cupressus macrocarpa Hartw.	T	0.35 ± 0.15(s)	35 ± 5	(10);(15)	Chang 1954b (3)	600	7	0.37	0.97	9.7
Ginkgo biloba	T	7.5 ± 2.5	12 ± 1.2	(8 ± 5);(13 ± 8)	This study (1, 2, 3)	420	5.8	2.7	5.4	156
Juniperus virginiana L.	T	0.35 ± 0.15(s)	13 ± 8	(5);(12.5 ± 2.5)	Chang 1954b (3)	250	4.1	0.14	0.58	15.6
Larix laricina (Du Roi) K. Koch	T	2.5 ± 0.5	15 ± 5	(11 ± 4);(20 ± 5)	Chang 1954b (3)	880	8.2	1.1	2.4	56
Larix occidentalis	T	3.5 ± 1.5	45 ± 15	(13 ± 5);(25 ± 10)	Chang 1954a (3)	1300	9.9	4.7	7.4	57.6
Libocedrus decurrens Torr.	T	0.90 ± 0.70(s)	50 ± 10	(15);(22.5 ± 2.5)	Chang 1954b (3)	1400	11	1.3	2.4	16.5
Picea abies (L.) Karst.	T	1.8 ± 0.6	45 ± 10	(8.1 ± 0.8);(13 ± 4)	Schulz & Behnke 1987 (3)	420	5.8	2.4	5	39.2
Picea abies ad fennica	T	1.7 ± 0.3	24 ± 2.4	(7.8 ± 1.9);(13.3 ± 2)	This study (1, 2, 3)	410	5.7	1.2	3.1	45.7
Picea engelmannii	T	2.1 ± 0.4	6 ± 0.6	(8.7 ± 1.4);(12.6 ± 1.4)	This study (1, 2, 3)	440	6	0.38	1.1	65.8
P. engelmannii Parry	T	2.3 ± 0.8	33 ± 8	(12.5);(16)	Chang 1954a (3)	800	8.2	2.3	4.5	47.6
Picea glauca (Moench) Voss	T	1.6 ± 0.3	23 ± 8	(7.5 ± 2.5);(10 ± 5)	Chang 1954b (3)	300	5	1.1	3	45.6
Picea mariana (Mill) B.S.P.	T	11 ± 5	10 ± 5	(11 ± 4);(20)	Chang 1954a (3)	880	8.2	3.3	6	210
Picea sitchensis	T	1.6 ± 0.3	15 ± 1.5	(13 ± 4);(19 ± 6)	This study (1, 2, 3)	990	9.1	0.72	1.5	34.6
Pinus banksiana Lamb.	T	3 ± 1	16 ± 7	(9 ± 4);(18 ± 8)	Chang 1954a (3)	650	6.9	1.4	3.3	71.9
Pinus contorta Dougl.	T	6 ± 2	45 ± 5	(9 ± 4);(12.5 ± 2.5)	Chang 1954a (3)	450	6.1	8.1	9.4	73
Pinus echinata Mill.	T	9 ± 2	25 ± 5	(12.5 ± 2.5);(20 ± 5)	Chang 1954b (3)	1000	9	6.8	10	140
Pinus elliottii Engelm.	T	21 ± 3	24 ± 6	(12.5);(20)	Chang 1954a (3)	1000	9	15	16	234
Pinus monticola Dougl.	T	9 ± 4	40 ± 10	(12.5 ± 2.5);(20 ± 5)	Chang 1954b (3)	1000	9	11	13	118
Pinus pinea	T	1.5 ± 0.5	16 ± 4	7.4	Esau 1969 (3)	170	7.4	3.8	2.2	48.1
Pinus pumila	T	6.4 ± 1.3	2.5 ± 0.25	(5.3 ± 1.1);(9.4 ± 1.8)	This study (1, 2, 3)	200	3.9	0.48	1.7	238
Pinus strobus	T	10 ± 2	20 ± 4	10.9 ± 1.0	Jensen et al. 2011 (1, 2, 3)	370	11	32	8.2	144
Pinus sylvestris var. NANA	T	6.0 ± 1.2	10 ± 1	(7.1 ± 1.0);(16.3 ± 2.3)	This study (1, 2, 3)	460	5.7	1.8	4.1	142
Pseudotsuga menziesii (Mirb.) Franco	T	2.8 ± 0.8	68 ± 8	(12.5 ± 2.5);(25)	Chang 1954b (3)	1200	9.6	5.7	8.7	44.5
Taxodium distichum (L.) Rich.	T	1.5 ± 0.5	33 ± 8	(8.8 ± 1.3);(25)	Chang 1954b (3)	880	7.3	1.5	3.2	33.9
Taxus baccata (female)	T	1.9 ± 0.4	13 ± 1.3	(5.2 ± 1.0);(11.3 ± 2.3)	This study (1, 2, 3)	240	4.1	0.74	2.2	60.6
Taxus brevifolia Nutt.	T	2 ± 1	12.5 ± 2.5	(15);(7.5)	Chang 1954a (3)	450	5.8	0.75	2.1	58.6
Thuja occidentalis L.	T	0.40 ± 0.10(s)	15 ± 5	(7.5);(15)	Chang 1954b (3)	450	5.8	0.18	0.57	13.4
Thuja plicata	T	0.23 ± 0.03(s)	15 ± 1.5	(6 ± 1.6);(10.8 ± 2.7)	This study (1, 2, 3)	260	4.5	0.1	0.42	9.87
Torreya californica Torr.	T	4 ± 1	20 ± 5	(12.5 ± 2.5);(20 ± 5)	Chang 1954a (3)	1000	9	2.4	4.5	78.1
Tsuga canadensis	T	1.8 ± 0.3	31	(7.5);(15)	Chang 1954a (3)	450	5.8	1.6	3.8	43.1

Table 2. *Continued*

| Species	Life form	l_{source} [cm] (1)	l_{trans} [m] (2)	SE geometry: a or $(a_t);(a_r)$ [μm] (3)	Reference	A [1000 μm²]	a [μm]	$G\,l_{source}\,l_{trans}$ [m²]	k [μm²]	u [μm s⁻¹]
Tsuga heterophylla	T	1.5 ± 0.3	30 ± 3	(14.8 ± 2.0);(23 ± 3)	This study (1, 2, 3)	1400	11	1.3	2.4	27.6
Tsuga heterophylla (Raf.) Sarg.	T	1.4 ± 0.9	60 ± 10	(6.3 ± 1.3);(11 ± 4)	Chang 1954b (3)	280	4.7	2.5	4.7	27.3
Angiosperms										
Acer platanoides	T	15 ± 3	12 ± 1.2	(7.0 ± 1.3);(9 ± 4)	This study (1, 2, 3)	250	4.6	5.4	6.1	178
Acer pseudoplatanus L.	T	11 ± 2	27 ± 3	9.1 ± 1.1	This study (1, 2, 3)	260	9.1	48	7.9	102
Acer saccharum Marsh	T	12 ± 4	30 ± 5	18 ± 8	Chang 1954a (3)	1000	18	58	13	156
Aesculus hippocastanum	T	25 ± 5	31 ± 3	14.1 ± 2.2	This study (1, 2, 3)	620	14	120	17	193
Alnus rubra Bong	T	11 ± 4	28 ± 8	23 ± 8	Chang 1954a (3)	1700	23	49	11	139
Anacyclus pyrethrum	H	1 ± 0.2	0.3 ± 0.06	2.1 ± 0.6	Jensen et al. 2011 (1, 2, 3)	14	2.1	0.048	0.11	132
Beta vulgaris	H	10 ± 2	0.30 ± 0.06	5 ± 1	Jensen et al. 2011 (1, 2, 3)	79	5	0.48	0.5	587
Betula alleghaniensis Britton	T	9 ± 3	18.5 ± 1.5	(15 ± 5);(23 ± 8)	Chang 1954a (3)	1400	11	5	7.6	144
Betula papyrifera Marsh.	T	8 ± 5	17.5 ± 1.5	(15 ± 5);(23 ± 8)	Chang 1954a (3)	1400	11	4.2	6.6	131
Cucumis sativus	H	10 ± 2	0.60 ± 0.12	6.3 ± 1.4	Jensen et al. 2011 (1, 2, 3)	120	6.3	0.96	0.8	466
Cucurbita maxima I	H	20 ± 4	4.0 ± 0.8	12.3 ± 2.7	Jensen et al. 2011 (1, 2, 3)	480	12	13	4.8	423
Cucurbita maxima II	H	20 ± 4	4.0 ± 0.8	16.6 ± 2.6	Jensen et al. 2011 (1, 2, 3)	870	17	13	4.2	370
Cucurbita pepo	H	30 ± 6	7.0 ± 1.4	40 ± 8	Jensen et al. 2011 (1, 2, 3)	5000	40	34	5.1	256
Ecbalium elaterium	H	20 ± 4	3.0 ± 0.6	15 ± 3	Jensen et al. 2011 (1, 2, 3)	710	15	9.6	3.5	409
Eragostis plana	H	10 ± 2	0.2 ± 0.04	3.0 ± 0.2	Jensen et al. 2011 (1, 2, 3)	28	3	0.32	0.42	733
Festuca arundinacea	H	5 ± 1	0.30 ± 0.06	3.0 ± 0.6	Jensen et al. 2011 (1, 2, 3)	28	3	0.24	0.35	404
Glycine max	H	10 ± 2	0.40 ± 0.08	3.7 ± 1.0	Jensen et al. 2011 (1, 2, 3)	43	3.7	0.64	0.66	580
Gossypium barbadense	S	15 ± 3	1.5 ± 0.3	11 ± 2.2	Jensen et al. 2011 (1, 2, 3)	380	11	3.6	1.8	420
Heracleum mantegazzianum	H	20 ± 4	2.0 ± 0.4	9 ± 2	Jensen et al. 2011 (1, 2, 3)	250	9	6.4	3.1	541
Liquidambar styraciflua L.	T	13 ± 6	28 ± 8	20 ± 5	Chang 1954a (3)	1300	20	58	13	167
Nyssa sylvatica Marsh.	T	9 ± 4	23 ± 3	20 ± 5	Chang 1954a (3)	1300	20	33	8.6	130
Platanus occidentalis L.	T	13 ± 7	35 ± 5	25 ± 5	Chang 1954a (3)	2000	25	73	15	148
Populus tremuloides Michx.	T	5 ± 2	22.5 ± 2.5	20 ± 5	Chang 1954a (3)	1300	20	18	5.1	78.7
Robinia pseudoacacia	T	3 ± 0.6	40 ± 8	10 ± 1	Jensen et al. 2011 (1, 2, 3)	310	10	19	6.1	53.6
Sabal palmetto	T	50 ± 10	20 ± 4	16.5 ± 1.7	Jensen et al. 2011 (1, 2, 3)	860	16	160	22	381
Salix nigra Marshall	T	10 ± 5	20 ± 10	25 ± 5	Chang 1954a (3)	2000	25	32	7.3	127
Solanum lycopersicum	H	10 ± 2	0.4 ± 0.08	5.2 ± 0.8	Jensen et al. 2011 (1, 2, 3)	85	5.2	0.64	0.63	548
Tilia americana	T	10 ± 2	20 ± 4	15 ± 1.5	Jensen et al. 2011 (1, 2, 3)	710	15	32	9	158
Tradescantia virginiana	H	2 ± 0.4	0.10 ± 0.02	1.2 ± 0.4	Jensen et al. 2011 (1, 2, 3)	5	1.2	0.032	0.087	303
Ulmus americana L.	T	14 ± 7	32.5 ± 2.5	25	Chang 1954a (3)	2000	25	73	15	159
Vitis vinifera	T	10 ± 2	20 ± 4	18 ± 4	Jensen et al. 2011 (1, 2, 3)	1000	18	32	8.7	153
Yucca flaccida	S	50 ± 10	1.0 ± 0.2	10 ± 2	Jensen et al. 2011 (1, 2, 3)	310	10	8	3.6	1250

The 13 field samples were collected at the Charlottenlund Arboretum, Denmark, on 30 April 2011 and at the University of Copenhagen, Faculty of Life Sciences in Frederiksberg, Denmark, on 27 May 2011. At a stem height of around 1.3 m, the outer bark was removed in an area large enough to cut out 1 cm by 2 cm samples of the inner bark, including the current-year phloem. Tree height, l_{trans}, of the sampled tree was measured as the distance between the ground and the top of the tree (Fig. 1b). Average leaf length, l_{source}, was determined by measuring the length of the leaf blade or needle without petiole (Fig. 1b). All trees were mature.

The bark samples were cross-sectioned with a razor blade and bright-field images of the inner bark were taken with a Leica SP5X confocal microscope. SE diameters (without cell wall) of the current-year phloem were determined manually with the help of LAS AF Lite (Leica, Wetzlar, Germany) or Velocity (Perkin Elmer, Wellesley, MA, USA) software. A minimum of 24 SEs were measured per plant on two to four sections. Only clearly differentiated SEs were selected, as identified by the absence of visible cellular content, their specific shape and their size in relation to that of other cell types (see Fig. 1d,e).

RESULTS

A comparison between the anatomical phloem data from gymnosperm and angiosperm species given in Table 2 reveals several features. As shown in Fig. 2, there appears to be no clear correlation neither between stem size l_{trans} and leaf size l_{source} (Fig. 2a) nor between leaf size l_{source} and single stem SE cross-sectional area A (Fig. 2c). Interestingly, as shown in Fig. 2b, the SE area A is seen to scale with plant height l_{trans} in herbaceous plants. Regression analysis yields $A \propto l_{\text{trans}}^{1.3 \pm 0.1}$ ($r^2 = 0.90$; $N = 13$; $\alpha_{\text{RMA}} = 1.4 \pm 0.1$), but we find no increase in SE area in plants higher than 5 m. Here, we follow Niklas (1994) and give scaling exponents obtained by least square ($\alpha_{\text{LS\_}} = 1.3 \pm 0.1$) and reduced major axis ($\alpha_{\text{RMA\_}} = 1.4 \pm 0.1$) regressions for a dataset with N plants and correlation coefficient r. SE area of angiosperm as well as gymnosperm trees is seen to saturate above $l_{\text{trans}} = 5$ m near the value $A \simeq 10^{-9}$ m$^2 = 10^3\ \mu m^2$.

Figure 2. Plots of anatomical phloem data for 32 angiosperm and 38 gymnosperm species. (a) Leaf size l_{source} plotted as a function of stem size l_{trans}. (b) Sieve element (SE) area A plotted as a function of stem size l_{trans}. (c) SE area A plotted as a function of leaf size l_{source}. In (b), the SE area A saturates near $l_{\text{stem}} = 5$ m at the value $= 10^{-9}$ m$^2 = 10^3\ \mu m^2$. Dashed line in (b) through the data points for herbaceous species is the regression curve obtained from least square regression analysis, $A \propto l_{\text{stem}}^{1.3 \pm 0.1}$ ($r^2 = 0.90$; $N = 13$; $\alpha_{\text{RMA}} = 1.4 \pm 0.1$). The conductivity k was calculated from Eqns 3, 9 and A4. In the plot we assume that the viscosity η and membrane permeability L_p do not scale with plant height. Parameters used are $L_p = 5 \times 10^{-14}$ m/(Pa s) and $\eta = 2 \times 10^{-3}$ Pa s (Thompson & Holbrook 2003b). Symbol legend: angiosperm trees (open circle), angiosperm herbs (black dot), angiosperm shrubs (grey dot), gymnosperm trees (open square), gymnosperm trees with scales (open triangle).
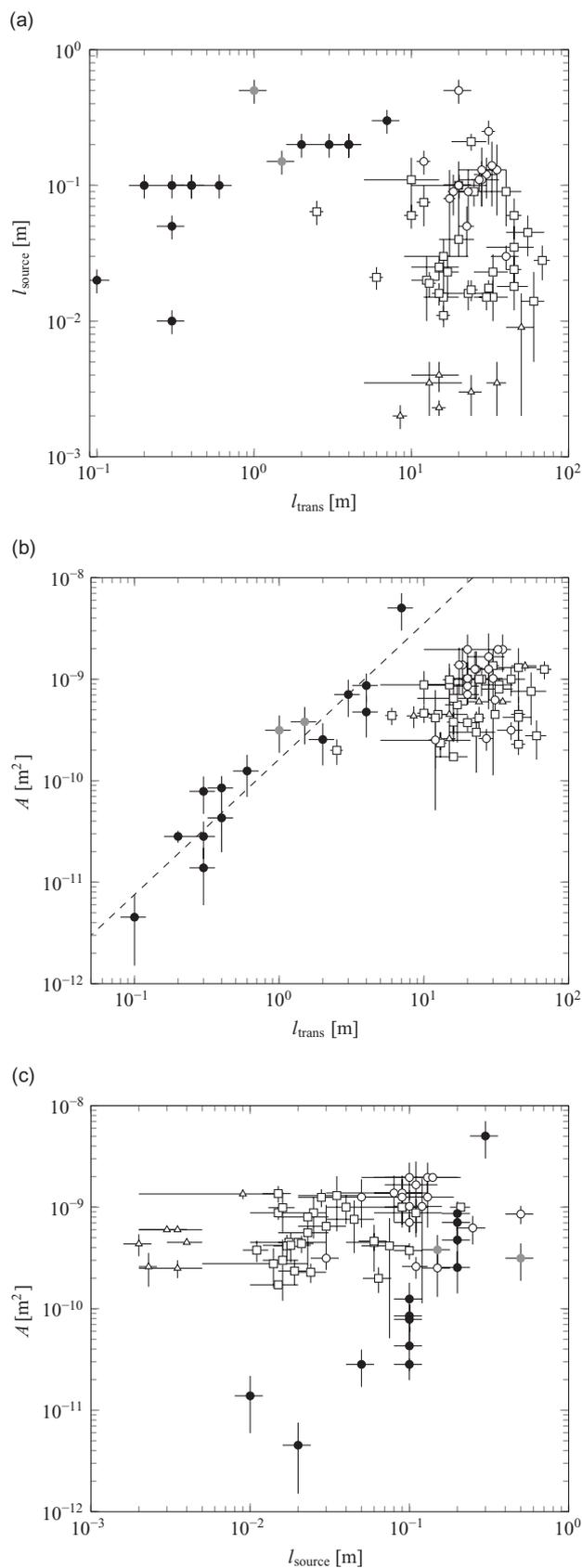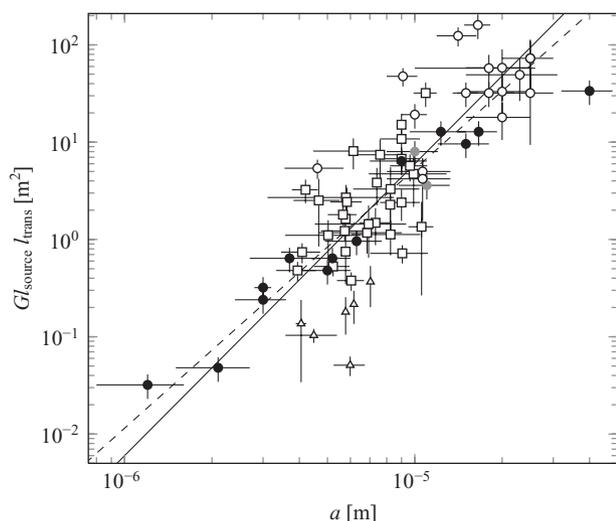
Figure 3. Plot of $Gl_{source}l_{trans}$ as a function of the effective osmotic radius a. The plants are hydraulically optimized for rapid translocation in the phloem if the points fall on the solid black line (slope 3), as predicted by Eqn 8. The dashed line is the regression curve obtained from least square regression analysis, $l_{source}l_{trans} \propto a^{2.7\pm0.10}$ ($r^2 = 0.69$; $N = 70$; $\alpha_{RMA} = 3.3 \pm 0.2$) Symbol legend: angiosperm trees (open circle), angiosperm herbs (black dot), angiosperm shrubs (grey dot), gymnosperm trees (open square), gymnosperm trees with scales (open triangle).

A comparison between the experimental data and the optimality prediction of Eqn 7 is shown in Fig. 3. We observe that many angiosperms as well as gymnosperms fall on the predicted scaling line, suggesting that both taxa are optimized for rapid translocation in the phloem. Regression yields $l_{source}l_{trans} \propto a^{2.7\pm0.2}$ ($r^2 = 0.69$; $N = 70$; $a_{RMA} = 3.3 \pm 0.2$) for 32 angiosperms and 38 gymnosperms, close to the predicted value 3, cf. Eqn 8. A similar scaling exponent ($a_{LS} = 2.6 \pm 0.3$) was found by Jensen *et al.* (2011) for a much smaller dataset (19 angiosperms, 1 gymnosperm). To quantify whether $\alpha_{LS} = 2.7 \pm 0.2$ and $\alpha_{RMA} = 3.3 \pm 0.2$ differ significantly from the predicted value 3.0, we calculate the test statistic t-values $t_{LS} = \frac{|\alpha_{LS} - 3.0|}{\sigma_{LS}} = 1.5$ and $t_{RMA} = \frac{|\alpha_{RMA} - 3.0|}{\sigma_{RMA}} = 1.5$, see, for example, Taylor (1997). The probability of obtaining an answer that differs from 3.0 by $t = 1.5$ or more standard deviations is found from the normal error integral to be 13.4%. We therefore conclude that there is insufficient evidence to indicate a difference between the obtained and predicted scaling exponents. These results indicate that even though, as discussed in the Introduction, gymnosperms have significantly lower translocation speeds than found in angiosperms, the size of their SE is equally optimized for efficient translocation.

The conductivity k is plotted as a function of stem length l_{trans} in Fig. 4. The figure indicates that the conductivity in herbaceous plants scales with the height of the plant, and regression yields $k_{herb} \propto l_{trans}^{0.97\pm0.10}$, ($r^2 = 0.90$; $N = 13$; $\alpha_{RMA} = 1.02 \pm 0.10$). Angiosperm and gymnosperm trees show similar scalings but tend to have relatively lower

conductivities compared with herbaceous plants. If we compare within trees, we find that gymnosperms have lower conductivities than angiosperm trees of similar height.

## DISCUSSION

Optimum velocity scaling law

The fact that the scaling relationship between the structural parameters of phloem transport, leaf length, stem length and SE radius is the same in gymnosperms as in angiosperms (Fig. 3) is a strong indication that gymnosperms employ the same basic mechanism for phloem transport. Active transport facilitation, which has been hypothesized to contribute to phloem transport in trees (Lang 1979; Aikman 1980) and especially gymnosperms (Kollmann 1975; Liesche *et al.* 2011), would likely have altered the scaling relationship. For example, for the relay mechanism proposed by Lang (Lang 1979), where the translocation pathway is split into shorter, hydraulically isolated segments, one would expect to find narrower SEs if the osmotic pumping mechanism was optimized in a similar way to that described in the present manuscript.

Ernst Münch explicitly included gymnosperms in his proposition of the pressure-flow hypothesis, providing evidence for the validity of the mechanism in this plant group by relating seasonal stem growth to sugar transport capacity in conifers (Münch 1930). Other authors excluded a contribution by energy-dependent transporters along the stem by cooling experiments (Watson 1980) and demonstrated the direct correlation of leaf carbohydrates with sink activity as expected for a system driven by hydrostatic pressure
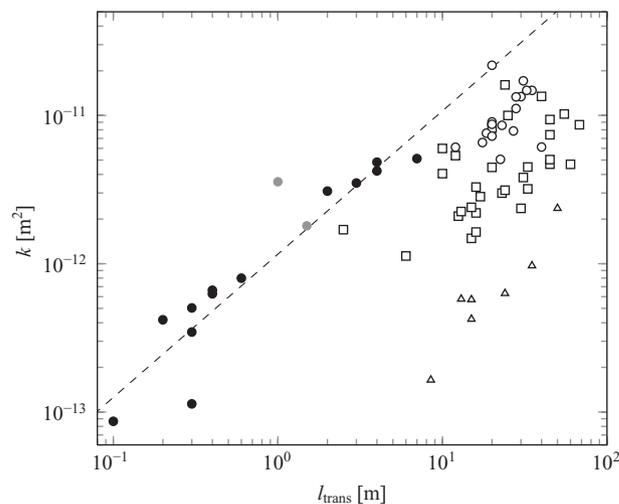
Figure 4 Plot of the conductivity k as a function of stem length l_{trans}.
The dashed line through the data points for herbaceous species is the regression curve obtained from least square regression analysis, $k_{herb} \propto l_{trans}^{0.97\pm0.10}$ ($r^2 = 0.90$; $N = 13$; $\alpha_{RMA} = 1.02 \pm 0.10$). Symbol legend: angiosperm trees (open circle), angiosperm herbs (black dot), angiosperm shrubs (grey dot), gymnosperm trees (open square), gymnosperm trees with scales (open triangle).
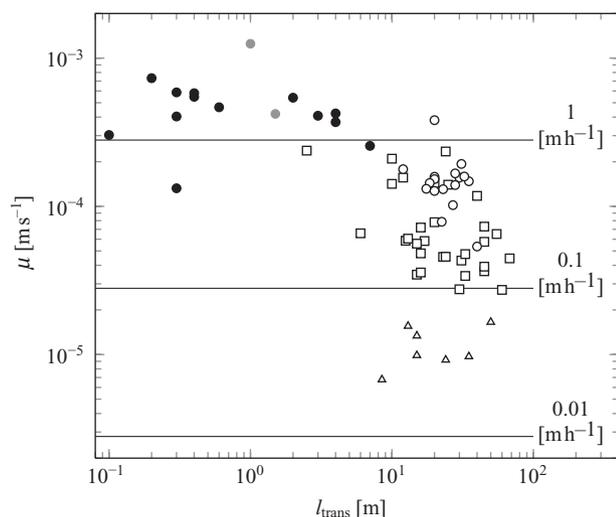
Figure 5. Plot of calculated flow velocity u determined as a function of stem length l_{trans} determined from Eqn 1. In the plot, we assume that osmotic pressure Δp, viscosity η and membrane permeability L_p do not scale with plant height. The solid lines indicate the location of 0.01, 0.1 and 1 m h^{-1} levels. Parameters used are $L_p = 5 \times 10^{-14}$ m s^{-1} Pa^{-1}, $\eta = 2$ mPa and $\Delta p = 0.7$ MPa (Thompson & Holbrook 2003b; Turgeon 2010). Symbol legend: angiosperm trees (open circle), angiosperm herbs (black dot), angiosperm shrubs (grey dot), gymnosperm trees (open square), gymnosperm trees with scales (open triangle).

potential (Sevanto *et al.* 2003). The anatomical optimization of gymnosperm phloem for rapid transport, shown here, corroborates the assumption that gymnosperms employ the Münch mechanism for phloem transport.

Although the experimental data support the optimality hypothesis, a number of species divert from the general scaling behaviour. The scaling pre-factor L_p (Eqn 7) is the product of the membrane permeability L_p and sugar solution viscosity η which in the present analysis has been assumed equal for all species. These may, however, vary slightly among species (Thompson & Holbrook 2003b), in part explaining the vertical deviations from the scaling law. In addition to this, a subgroup of gymnosperms with scale-like leaves lies below the predicted scaling line and also diverts from the other gymnosperms in the following analysis (Figs 3–5). This might be due to our definition of l_{source} as the anatomical unit of a leaf or needle which does not necessarily correspond to the physiological unit. In case of the scale-like leaves, which are usually less than 2 mm long, the physiological unit might consist of several individual scales. However, for the sake of consistency we did not change the definition of l_{source} for scale-like leaves in our analysis.

All data examined in the present paper were taken from mature plants. It is an open question whether plants are hydraulically optimized during growth, moving along the solid black line in Fig. 3, or if they have the same SE radius in all phases of growth, thus moving along a vertical axis. The authors will address this in a future publication.

Flow velocity and conductivity in the phloem

The resistor model introduced in the present paper provides a framework for understanding many qualitative and quantitative features of long-distance phloem transport observed in plants. For example, the specific flow conductivity k (Eqn 8) was found to scale with plant height as $k_{herb} \propto l_{trans}^{0.97\pm0.10} (r^2 = 0.90; N = 13; \alpha_{RMA} = 1.02 \pm 0.10)$, for herbaceous angiosperms. Another important result was that the conductivity was significantly lower in gymnosperm trees compared with angiosperm trees of similar height (Fig. 4). This may in part explain why the observed translocation speeds in gymnosperms are slower than in angiosperms. The velocity u calculated from the conductivity k (see Eqn 8) is plotted as a function of stem length l_{trnas} in Fig. 5. Here, we assume that the pressure drop Δp and viscosity η do not scale with plant height (Turgeon 2010), and that the membrane permeability L_p does not vary among the species. Our calculations predict that herbaceous species translocate with speeds of about 1 m h^{-1}, angiosperm trees with speeds in the range 0.1–1 m h^{-1} and gymnosperm trees in the range 0.01–1 m h^{-1}, mostly in agreement with earlier experimental results (Crafts & Crisp 1971; Thompson *et al.* 1979). Consistent with our findings for the conductivity, the flow speed predicted in gymnosperms is significantly lower than in angiosperm trees of comparable height.

Our results indicate that the slower phloem translocation is the result of the different SE anatomy, that is, the smaller effective radius, which generally reduces the conductivity in comparison with angiosperms of similar height (see Fig. 4). The sieve plate resistance, not considered here, might have an additional negative effect on sap flow velocity because of the narrower pore structure (Kollmann 1975; Schulz 1992). Gymnosperms are, however, as efficient as angiosperms in terms of utilizing the full potential of the osmotic Münch mechanism, as evidenced by the range of sieve element radii developed in evolution.

The slow phloem transport in gymnosperms might be offset by a larger number of SEs to accommodate a sufficient volume (Münch 1930; Schulz 1990) at least in mature conifers which show seasonal growth comparable to angiosperm trees (Münch 1930; Bond 1989). Aspects of carbon partitioning such as low diurnal variation in export (Yang *et al.* 2002; Bansal & Germino 2009) might contribute to the absolute transport volumes of gymnosperms. The big carbon reserves in all plant organs of gymnosperms guarantee a sufficient supply even when transport is slow (Ericsson & Persson 1980; Cranswick, Rook & Zabkiewicz 1987; Webb & Kilpatrick 1993).

SE cross-sectional area

The relation between plant height and stem SE cross-sectional area was found to be profoundly different between herbaceous plants and trees (Fig. 2b). In herbaceous plants, the SE area was found to scale with plant height as $A_{herb} \propto l_{trans}^{1.3\pm0.1} (r^2 = 0.90; N = 13; \alpha_{RMA} = 1.4 \pm 0.1)$.

The SE area in trees was found to be mostly larger than in herbs, but limited to values around 10^3 μm^2 and appears to be independent of plant height in both angiosperm and gymnosperm species.

The SE cross-sectional area might be limited by the effectiveness of SE maintenance. Mature SEs of angiosperms are functionally dependent on ontogenetically related companion cells, to which they are connected via specialized plasmodesmata. With larger SE diameter, the interface might get too small for efficient turnover of proteins and lipids from the companion cells. Gymnosperm SEs might well be even more limited with respect to the maximal cross-sectional area, as the Strasburger cells, they are associated with, have a much smaller contact interface with SEs than angiosperm companion cells have (Schulz 1990).

In spite of this similarity in SE area, we find that the conductivity k is significantly smaller in gymnosperms than angiosperms of similar height. The reason for this is that cuboidal cells, often found in gymnosperm trees, offer larger hydraulic resistance to flow than a cylindrical cell of equal cross-sectional area A. For a square cross section ($a_r = a_t$) the increase is 13%, while for rectangular cross section with $a_r = 1/2a_t$, the ratio typically found in the data examined in the present paper, the increase is 39%.

General

The central finding of this work is that both gymnosperm and angiosperm plants are geometrically optimized for rapid translocation in the phloem and that the flow conductivity is significantly lower in gymnosperms compared with angiosperms of similar height.

The results demonstrate universal optimization of the phloem in seed plants for a transport compatible with the Münch mechanism and contribute to our understanding of carbon allocation in trees, especially in gymnosperms.

ACKNOWLEDGMENTS

REFERENCES

Aikman D.P. (1980) Contractile proteins and hypotheses concerning their role in phloem transport. *Canadian Journal of Botany. Journal Canadien De Botanique* **58,** 826–832.

Bansal S. & Germino M.J. (2009) Temporal variation of nonstructural carbohydrates in montane conifers: similarities and differences among developmental stages, species and environmental conditions. *Tree Physiology* **29,** 559–568.

Becker P., Tyree M.T. & Tsuda M. (1999) Hydraulic conductances of angiosperms versus conifers: similar transport sufficiency at the whole-plant level. *Tree Physiology* **19,** 445–452.

Bond W.J. (1989) The tortoise and the hare – ecology of angiosperm dominance and gymnosperm persistence. *Biological Journal of the Linnean Society. Linnean Society of London* **36,** 227–249.

Bruus H. (2008) *Theoretical Microfluidics*. Oxford University Press, Oxford, OH, USA.

Carlquist S.J. (1975) *Ecological Strategies of Xylem Evolution*. University of California Press, Berkeley and Los Angeles, CA, USA.

Chang Y.-P. (1954a) *Anatomy of Common North American Pulpwood Barks. Tappi Monograph Series*. Vol. **14**. Technical Association of the Pulp and Paper Industry, New York, NY, USA.

Chang Y.-P. (1954b) *Bark Structure of North American Conifers*. U.S. Department of Agriculture, Washington, DC, WA, USA.

Crafts A.S. (1939) The relation between structure and function of the phloem. *American Journal of Botany* **26,** 172–177.

Crafts A.S. & Crisp C. (1971) *Phloem Transport in Plants*. W.H. Freeman and Company, San Francisco, CA, USA.

Cranswick A., Rook D. & Zabkiewicz J. (1987) Seasonal changes in carbohydrate concentration and composition of different tissue types of *Pinus radiata* trees. *New Zealand Journal of Forestry Science* **2/3,** 229–245.

Dannoura M., Maillard P., Fresneau C., *et al.* (2011) In situ assessment of the velocity of carbon transfer by tracing 13C in trunk CO(2) efflux after pulse labelling: variations among tree species and seasons. *New Phytologist* **190,** 181–192.

Ericsson A. & Persson H. (1980) Seasonal changes in starch reserves and growth of fine roots of 20-year-old Scots pines. *Ecological Bulletins* **32,** 239–250.

Esau K. (1969) *The Phloem* Vol. 5, Part 2. Gebr. Borntraeger, Stuttgart, Germany.

Evert R.F. (1984) Comparative structure of phloem. In *Contemporary Problems in Plant Anatomy* (eds R.A. White & W.C. Dickinson), pp. 145–234. Academic Press, Orlando, FL, USA.

Holbrook N.M. & Zwieniecki M.A. (2005) *Vascular Transport in Plants*. Elsevier Academic Press, San Diego, CA, USA.

Jensen K.H., Rio E., Hansen R., Clanet C. & Bohr T. (2009) Osmotically driven pipe flows and their relation to sugar transport in plants. *Journal of Fluid Mechanics* **636,** 371–396.

Jensen K.H., Lee J., Bohr T., Bruus H., Holbrook N.M. & Zwieniecki M.A. (2011) Optimality of the Münch mechanism for translocation of sugars in plants. *Journal of the Royal Society Interface* **8,** 1155–1165.

Knoblauch M. & Peters W.S. (2010) Münch, morphology, microfluidics – our structural problem with the phloem. *Plant, Cell & Environment* **33,** 1439–1452.

Kollmann R. (1975) Sieve element structure in relation to function. In *Phloem Transport* (eds S. Aronoff, J. Dainty, P. Gorham, L. Srivastava & C. Swanson), pp. 225–242. Plenum Press, New York, NY, USA.

Lang A. (1979) Relay mechanism for phloem translocation. *Annals of Botany* **44,** 141–145.

Liesche J., Martens H.J. & Schulz A. (2011) Symplasmic transport and phloem loading in gymnosperm leaves. *Protoplasma* **248,** 181–190.

Millburn J. & Kallarackal J. (1989) Physiological aspects of phloem translocation. In *Transport of Photoassimilates* (eds D. Baker & J. Milburn), pp. 264–305. John Wiley & Sons, New York, NY, USA.

Minchin P.E.H., Thorpe M.R. & Farrar J.F. (1993) A simple mechanistic model of phloem transport which explains sink priority. *Journal of Experimental Botany* **44,** 947–955.

Mullendore D.L., Windt C.W., Van As H. & Knoblauch M. (2010) Sieve tube geometry in relation to phloem flow. *The Plant Cell* **22,** 579–593.

Münch E. (1930) *Die Stoffbewegungen in der Pflanze*. Gustav Fischer, Jena, Germany.

Nielsen C.H. (2010) Major intrinsic proteins in biomimetic membranes. *Advances in Experimental Medicine and Biology* **679,** 127–142.

Niklas K. (1994) *Plant Allometry: The Scaling of Form and Process*. The University of Chicago Press, Chicago, IL, USA.

Pickard W.F. & Abraham-Shrauner B. (2009) A 'simplest' steady-state Münch-like model of phloem translocation, with source and pathway and sink. *Functional Plant Biology* **36,** 629–644.

Plain C., Gerant D., Maillard P., Dannoura M., Dong Y.W., Zeller B., Priault P., Parent F. & Epron D. (2009) Tracing of recently assimilated carbon in respiration at high temporal resolution in the field with a tuneable diode laser absorption spectrometer after in situ (CO2)-C-13 pulse labelling of 20-year-old beech trees. *Tree Physiology* **29,** 1433–1445.

Rennie E.A. & Turgeon R. (2009) A comprehensive picture of phloem loading strategies. *Proceedings of the National Academy of Sciences of the United States of America* **106,** 14162–14167.

Schulz A. (1990) Conifers. In *Comparative Structure, Induction and Development* (eds H.-D. Behnke & R.D. Sjolund), pp. 63–88. Springer Verlag, Berlin, Heidelberg, Germany; New York, NY, USA.

Schulz A. (1992) Living sieve cells of conifers as visualized by confocal, laser-scanning fluorescence microscopy. *Protoplasma* **166,** 153–164.

Schulz A. & Behnke H.-D. (1987) *Feinbau und Differenzierung des Phloems von Buchen, Fichten und Tannen aus Waldschadensge-bieten*. Abschlußbericht des Forschungsprojekts. Kernforschung-szentrum Karlsruhe – PEF-Berichte 16.

Sevanto S., Vesala T., Peramaki M. & Nikinmaa E. (2003) Sugar transport together with environmental conditions controls time lags between xylem and stem diameter changes. *Plant, Cell & Environment* **26,** 1257–1265.

Taylor J.R. (1997) *An Introduction to Error Analysis: The Study of Uncertainties in Physical Measurements*. University Science Books, Sausalito, CA, USA.

Thompson M.V. & Holbrook N.M. (2003a) Application of a single-solute non-steady-state phloem model to the study of long-distance assimilate transport. *Journal of Theoretical Biology* **220,** 419–455.

Thompson M.V. & Holbrook N.M. (2003b) Scaling phloem transport: water potential equilibrium and osmoregulatory flow. *Plant, Cell & Environment* **26,** 1561–1577.

Thompson R.G., Fensom D.S., Anderson R.R., Drouin R. & Leiper W. (1979) Translocation of C-11 from leaves of *Helianthus, Heracleum, Nymphoides, Ipomoea, Tropaeolum, Zea, Fraxinus, Ulmus, Picea,* and *Pinus* – comparative shapes and some fine-structure profiles. *Canadian Journal of Botany. Journal Canadien De Botanique* **57,** 845–863.

Turgeon R. (2010) The puzzle of phloem pressure. *Plant Physiology* **154,** 578–581.

Watson B.T. (1980) Effect of cooling on the rate of phloem trans-location in the stems of 2 gymnosperms, *Picea sitchensis* and *Abies procera*. *Annals of Botany* **45,** 219–223.

Webb W.L. & Kilpatrick K.J. (1993) Starch content in Douglas fir – diurnal and seasonal dynamics. *Forest Science* **39,** 359–367.

Willenbrink J. & Kollmann R. (1966) Über den Assimilattransport im Phloem von *Metasequoia*. *Zeitschrift für Pflanzenphysiologie* **55,** 42–53.

Windt C.W., Vergeldt F.J., De Jager P.A. & Van As H. (2006) MRI of long-distance water transport: a comparison of the phloem and xylem flow characteristics and dynamics in poplar, castor bean, tomato and tobacco. *Plant, Cell & Environment* **29,** 1715–1729.

Yang W.Q., Murthy R., King P. & Topa M.A. (2002) Diurnal changes in gas exchange and carbon partitioning in needles of fast- and slow-growing families of loblolly pine (*Pinus taeda*). *Tree Physiology* **22,** 489–498.

APPENDIX A: MATHEMATICAL MODEL

Rectangular SEs

For rectangular SEs, we have for the resistances in Eqn 2 that

$$R_{\text{source}} = \frac{1}{4(a_r + a_t)L_p l_{\text{source}}}, \tag{A1}$$

$$R_{\text{trans}} = \frac{3}{4}\frac{\eta l_{\text{trans}}}{a_r^3 a_t}\left(1 - \sum_{n,\text{odd}}\frac{1}{n^5}\frac{192}{\pi^5}\frac{a_r}{a_t}\tanh\left(\frac{n\pi a_t}{a_r}\right)\right)^{-1} \tag{A2}$$
$$\simeq \frac{3}{4}\frac{\eta l_{\text{trans}}}{a_r^3 a_t}\left(1 - 0.63\left(\frac{a_r}{a_t}\right)\right)^{-1},$$

$$R_{\text{sink}} = \frac{1}{4(a_r + a_t)L_p l_{\text{sink}}}, \tag{A3}$$

The error introduced by the approximation made in Eqn A2 depends on the aspect ratio $\delta = \frac{a_t}{a_r}$. For $\delta = 1$ it is 13%, while for $\delta = 2$ it is down to 0.2%, see, for example, Bruus (2008). Given the data given in Table 2, we find that δ is approximately constant and take on values in the range $\delta \simeq 1.5 - 2$. The shape of the sieve elements depends on the shape of the cambial initials which also give rise to the xylem tracheary elements (Esau 1969; Carlquist 1975). We speculate that this ratio of cell size is influenced by physi-ological and mechanical constrains to the xylem cells. In addition, divisions during sieve element differentiation as seen in many angiosperm species do not seem to be common in gymnosperms (Esau 1969).

With the expression for the velocity given in Eqns A1–A3, we write the flow velocity u, cf. Eqn 3, as

$$\frac{u(a_r, l_{\text{source}}, l_{\text{trans}}, l_{\text{sink}})\delta}{\Delta p L_p(1+\delta)} = \frac{a_r^2 l_{\text{source}}l_{\text{sink}}}{W l_{\text{source}}l_{\text{trans}}l_{\text{sink}} + a_r^3(l_{\text{source}} + l_{\text{sink}})}, \tag{A4}$$

where $W = 3L_p\eta(1+\delta)/(\delta - 0.63)$. As in Eqn 4, this has a maximum when

$$a_r^{*3} = \frac{2W l_{\text{source}}l_{\text{trans}}l_{\text{sink}}}{l_{\text{source}} + l_{\text{sink}}} \tag{A5}$$

Under the assumption that $l_{\text{source}} = l_{\text{sink}}$ this corresponds to

$$a_r^{*3} = \frac{3L_p\eta(1+\delta)}{\delta - 0.63}l_{\text{source}}l_{\text{trans}} \tag{A6}$$

Defining the effective osmotic radius as $a = a_r\left(\frac{\delta - 0.63}{1+\delta}\right)^{1/3} = a_r\left(\frac{a_t - 0.63a_r}{a_r + a_t}\right)^{1/3}$, this can be written as

$$a^{*3} = 3L_p\eta l_{\text{source}}l_{\text{trans}}. \tag{A7}$$

APPENDIX B: THE PERMEABILITY LENGTH $L_p\eta$

In the expression for the optimized radius (Eqn 8), the product $L_p\eta$ of the membrane permeability and viscosity of the phloem occurs. This is a microscopic length scale having to do with the structure of the semipermeable membrane. Let us think of the membrane as consisting of N pores of a hydrodynamic radius ρ and length κ. With Poiseuille flow, the volume flux Q across a given area Ω of the membrane driven by a pressure difference Δp_0 is then

$$Q = N \frac{\pi \rho^4}{8 \eta_w \kappa} \Delta p_0 \tag{B1}$$

where $\eta_w = 10^{-3}$ Pa s is the viscosity of the water that penetrates the membrane. The number of pores N is taken to be proportional to the area Ω:

$$N = \phi \frac{\Omega}{\pi \rho^2} \tag{B2}$$

where ϕ is the covering fraction, that is, the fraction of the membrane surface area covered by pores. Thus,

$$Q = \phi \Omega \frac{\rho^2}{8 \eta_w \kappa} \Delta p_0 = L_p \Omega \Delta p_0 \tag{B3}$$

from which we see that

$$L_p\eta = \phi \frac{\eta}{\eta_w} \frac{\rho^2}{8\kappa} \approx \phi \frac{\rho^2}{4\kappa} \tag{B4}$$

Taking $L_p \approx 5 \times 10^{-14}$ m s^{-1} Pa^{-1} and $\eta \approx 2 \times 10^{-3}$ Pa s $= 2\eta_w$ we get $L_p\eta \approx 10^{-16}$ m.

If we use typical values for the membrane thickness $\kappa \approx 5$ nm $= 5 \times 10^{-9}$ m and the pore radii $\rho \approx 2$ Å $= 2 \times 10^{-10}$ m, we must take $\phi \approx 0.5 \times 10^{-4}$.

Of course, for these atomic length scales the estimate using Poiseuille flow is invalid. Instead, we can compare to the estimates in the literature for the permeability of single aquaporins. In Nielsen (2010), a typical value of the permeability coefficient for single channel aquaporin is given as $p_f \approx 10^{-14}$ cm^3 s^{-1} $= 10^{-20}$ m^3 s^{-1}. This permeability can be written as

$$p_f = \pi \rho^2 \phi \left(\frac{RT}{V_w} \right) L_p \tag{B5}$$

$$= \phi \times 4\pi \times 10^{-20} \text{ m}^2 \times 1.3 \times 10^8 \text{ Pa} \times 5 \times 10^{-14} \text{ m s}^{-1} \text{ Pa}^{-1}$$

$$\approx \phi \times 10^{-24} \text{ m}^3 \text{ s}^{-1}$$

This is not far from $\phi \approx 10^{-4}$ as obtained above, showing that our estimate (B4) actually has the right order of magnitude.